

# Guided Diffusion for Fast Inverse Design of Density-based Mechanical Metamaterials

Yanyan Yang<sup>1,†</sup>, Lili Wang<sup>1,†</sup>, Xiaoya Zhai<sup>1,\*</sup>, Kai Chen<sup>2</sup>, Wenming Wu<sup>3</sup>, Yunkai Zhao<sup>1</sup>, Ligang Liu<sup>1</sup>, and Xiao-Ming Fu<sup>1,\*</sup>

<sup>1</sup>School of Mathematical Sciences, University of Science and Technology of China, Hefei, Anhui 230026, P.R. China

<sup>2</sup>Beijing Academy of Artificial Intelligence, Beijing 100190, P.R. China

<sup>3</sup>Hefei University of Technology, Hefei, Anhui 230026, P.R. China

\*Corresponding author(s): Xiaoya Zhai (xiaoyazhai@ustc.edu.cn); Xiao-Ming Fu (fuxm@ustc.edu.cn)

†These authors contributed equally to this work

## ABSTRACT

Mechanical metamaterial is a synthetic material that can possess extraordinary physical characteristics, such as abnormal elasticity, stiffness, and stability, by carefully designing its internal structure. To make metamaterials contain delicate local structures with unique mechanical properties, it is a potential method to represent them through high-resolution voxels. However, it brings a substantial computational burden. To this end, this paper proposes a fast inverse design method, whose core is an advanced deep generative AI algorithm, to generate voxel-based mechanical metamaterials. Specifically, we use the self-conditioned diffusion model, capable of generating a microstructure with a resolution of  $128^3$  to approach the specified homogenized tensor matrix in just 3 seconds. Accordingly, this rapid reverse design tool facilitates the exploration of extreme metamaterials, the sequence interpolation in metamaterials, and the generation of diverse microstructures for multi-scale design. This flexible and adaptive generative tool is of great value in structural engineering or other mechanical systems and can stimulate more subsequent research.

## Introduction

Architected metamaterials have sparked a new frontier in materials research, opening avenues for creating materials with tailored and unconventional functionalities. They allow precise control over various physical properties, such as mechanical strength<sup>1-3</sup>, Poisson's ratio<sup>4-8</sup>, and bulking behavior<sup>9-11</sup>. The surveys<sup>12-14</sup> summarize the research progress of mechanical metamaterials in detail.

The mechanical properties of metamaterials are determined by their geometries once the properties of the base material are given. Mathematically, geometry can be expressed in various forms, such as parametric function, implicit function, discrete mesh, and voxel representation. The voxel representation has two main advantages compared with other representations: (1) it is flexible to represent various geometries, thus possessing various mechanical properties, and (2) it is regular and simple, reducing the design difficulty of the metamaterial generation algorithm. Moreover, high-resolution metamaterials represented by a large number of voxels can have delicate local structures, thus showing exciting mechanical properties.

Voxel-based metamaterials are generally obtained by the topology optimization method to solve the inverse homogenization problem<sup>15</sup>. However, such a method has three limitations due to the large design space based on density. First, it still needs expensive computing resources and much computing time to complete high-resolution topology optimization, although various excellent algorithms have been proposed, such as multi-CPU framework<sup>16-18</sup>, GPU computation<sup>19-22</sup>, and adaptive mesh refinement<sup>23,24</sup>. Second, since the optimization problem is highly nonlinear and non-convex, the optimized metamaterials are closely related to the initialization. In practice, there is almost no rule to choosing initial metamaterials to be optimized with high stiffness (or even close to extreme values), and we can only make tedious trial and error. Third, due to the expensive computing burdens and the dependence on initial metamaterials, the generated metamaterials lack diversity to become with poor geometric connectivity, and it is challenging to create metamaterial sequences with extreme mechanical properties, thereby causing performance decreases in multi-scale design<sup>25,26</sup>.

Data-driven inverse design of mechanical metamaterials is a possible way to solve the limitations<sup>27</sup>. They can not only reverse design mechanical metamaterial cells<sup>28-31</sup> but also quickly assemble and generate multi-scale systems<sup>32,33</sup>. Specifically, since the goal of a deep generative AI model is highly similar to that of an inverse design algorithm, which is to generate a microstructure meeting specific requirements, deep generative AI models have been widely used to create microstructures<sup>34,35</sup>. In addition to the representation of models, datasets play a crucial role in this kind of algorithm. The existing microstructure

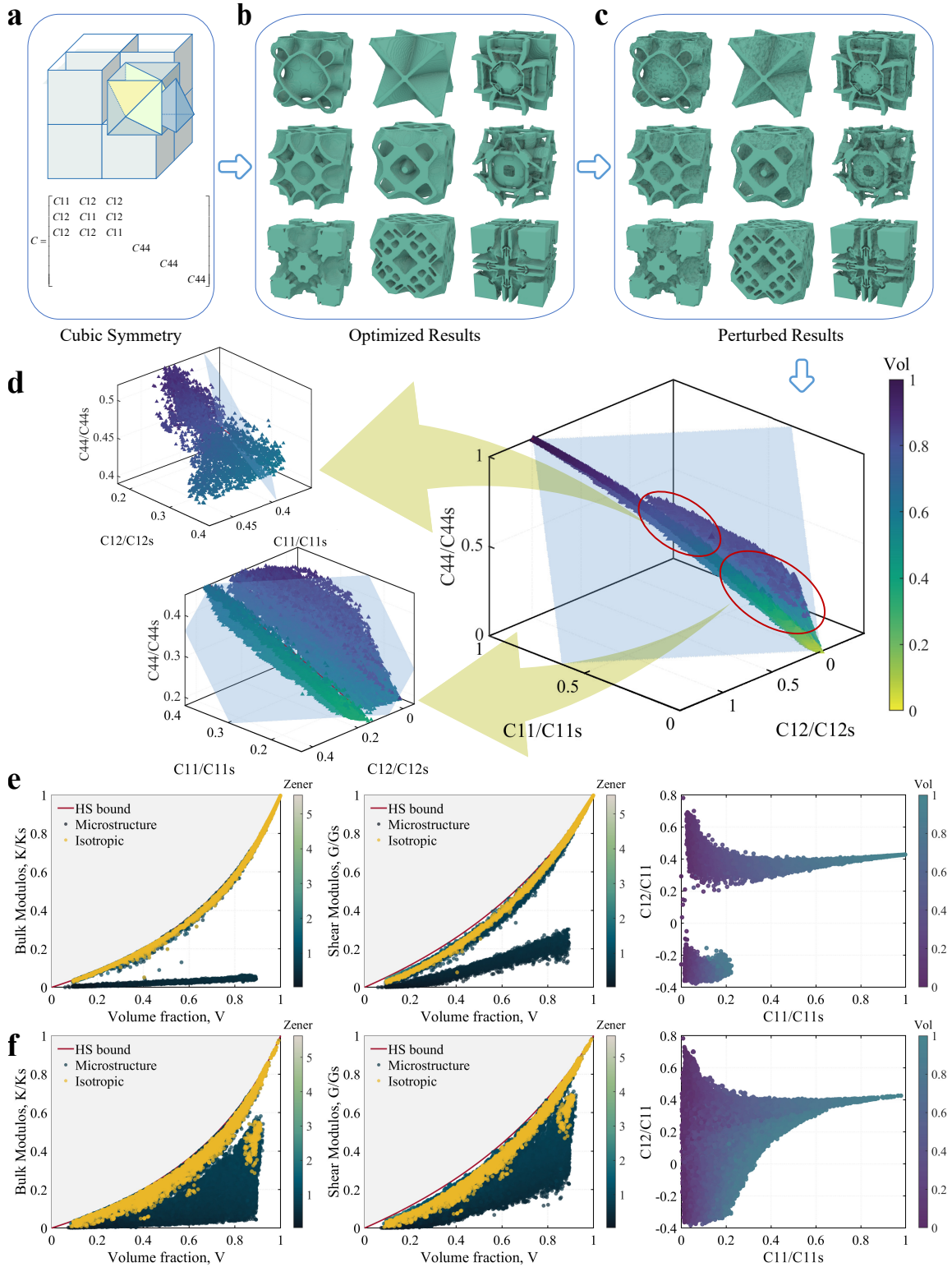


**Figure 1. Overview of the voxel-based metamaterial dataset.** **a** Cubic symmetry and elastic tensor matrix. **b** Optimized results. **c** Perturbation results. **d** Right: dataset in the attribute space, where the blue plane represents the isotropic plane. Top left: zoom-in views within the red circle, showing data on the isotropic plane. Bottom right: zoom-in views within the red circle, showing a slight gap in the dense part. **e** Bulk Modulus, shear Modulus, and Poisson's ratio of the optimized dataset. **f** Bulk Modulus, shear Modulus, and Poisson's ratio of the perturbed dataset

datasets mainly include two types: (1) low-resolution datasets using voxel representation<sup>36–38</sup> and (2) datasets with truss representation<sup>39–41</sup>. These existing datasets are imperfect. Currently, the majority of databases are configured in either a 2D or 3D truss structure<sup>36–38</sup>. The practical utility of a two-dimensional structure is constrained, and the expressive capacity of a three-dimensional bar structure is limited. Therefore, applying advanced data-driven methods and generating high-resolution voxel-based datasets with high property coverage to explore mechanical metamaterials remains promising.

We construct a voxel-represented mechanical metamaterial dataset at a high resolution, e.g.,  $128^3$ , with a comprehensive coverage of modulus variations. The complete dataset comprises optimized and perturbed data. The optimized data is obtained using the LIVE3D framework<sup>22</sup>, only requiring a single GPU. Specifically, the volume modulus, shear modulus, and Poisson’s ratio are optimization objectives, and the constrained volume fraction ranges from 0.2 to 0.9. Furthermore, isotropic constraints are added to optimize part of the microstructures. Thus, the optimized dataset includes both isotropic and anisotropic metamaterials. Subsequently, perturbation operations<sup>42</sup> are adapted to all data, resulting in a dataset featuring more diverse shapes and a broader coverage of modulus values.

This paper introduces a fast inverse design method to generate voxel-based mechanical metamaterials. Central to the technique is the use of the self-conditioned diffusion model (an advanced deep generative AI algorithm), which generates a microstructure with a resolution of  $128^3$  to approach the specified homogenized tensor matrix in just 3 seconds, substantially enhancing the efficiency of microstructure inverse design. It is successfully employed for efficient reverse design to facilitate the exploration of extreme metamaterials, sequence interpolation in metamaterials, and the generation of diverse microstructures. First, the diffusion model has been proven to be effective in generating initial microstructures for the subsequent traditional topology optimization. For example, we use the diffusion model to construct an initial microstructure with a negative Poisson’s ratio of  $-0.61$  and then realize the final extreme metamaterial with a negative Poisson’s ratio of  $-0.72$  through subsequent topology optimization. Second, according to the interpolation capability of the diffusion model, we generate a series of microstructure sequences that closely approach the theoretical upper limit. Finally, since the diffusion model is capable of generating geometrically diverse microstructures, making it more likely to find microstructures with high geometric connectivity and close to the target properties in multi-scale design.

## Results

### Metamaterials dataset

We construct a large-scale voxel-based metamaterial dataset under cubic symmetry constraints (Figure 1a). To create a sufficiently large design space for a voxel-represented metamaterial dataset, we establish microstructures at a resolution of  $128^3$  and subsequently store  $\frac{1}{8}$ -th of it due to the cubic symmetry constraint, i.e.,  $64^3$  microstructures. The representation is the basis for assembling a dataset incorporating a sizable assortment of voxel-based lattices, effectively capturing a broad range of mechanical properties. The construction process contains two phases.

1. First, we use the LIVE3D framework<sup>22</sup> to optimize a collection of metamaterials (Figure 1b). Specifically, trigonometric functions are adopted to cover various initial density fields. The basis functions of the initialization are  $\{\cos 2\pi kx, \sin 2\pi kx\}$  ( $0 < k \leq n$ ), where  $\mathbf{x} \in \mathbf{R}^3$  is the coordinate of the element’s center. We formulate the optimal model with the modulus as the objective function and the volume constraint.
2. Second, to make the dataset have a wide attribute coverage, we randomly perturb the optimized metamaterials (Figure 1c). Specifically, an iterative stochastic perturbation algorithm<sup>43</sup> generates novel structures by randomly deforming the surface of microstructures. Through iterative perturbation, the scope of the dataset is gradually expanded. The dataset’s volume fraction ranges from 0.1 to 1, while Poisson’s ratio values span from  $-0.4$  to  $0.8$ . This encompasses both isotropic and anisotropic metamaterials.

### Diffusion model framework

#### ML framework illustration

A diffusion model comprises both forward and reverse processes. In the forward process, Gaussian noise is incrementally introduced to the data point  $x_0$  until it evolves into pure Gaussian noise, denoted as  $x_T$ , which can be defined as follows:

$$x_t = \sqrt{\gamma_t}x_0 + \sqrt{1 - \gamma_t}\varepsilon, \quad (1)$$

where  $\varepsilon \sim \mathcal{N}(0, I)$ , and  $\gamma_t$  monotonically decrease from 1 to 0. The reverse process restores a Gaussian noise  $x_t$  to a data point  $x_0$  by denoising it step by step. At each step, the prediction of  $x_{t-1}$  from  $x_t$  is facilitated by a neural network, typically a U-Net, which predicts  $x_{t-1}$ ,  $\varepsilon$ , or  $x_0$ . In our work, we use a U-Net  $f(x_t, \tilde{x}_0, t, conditions)$  to map  $x_t$  to  $x_0$ , where  $\tilde{x}_0$  is an estimated of  $x_0$

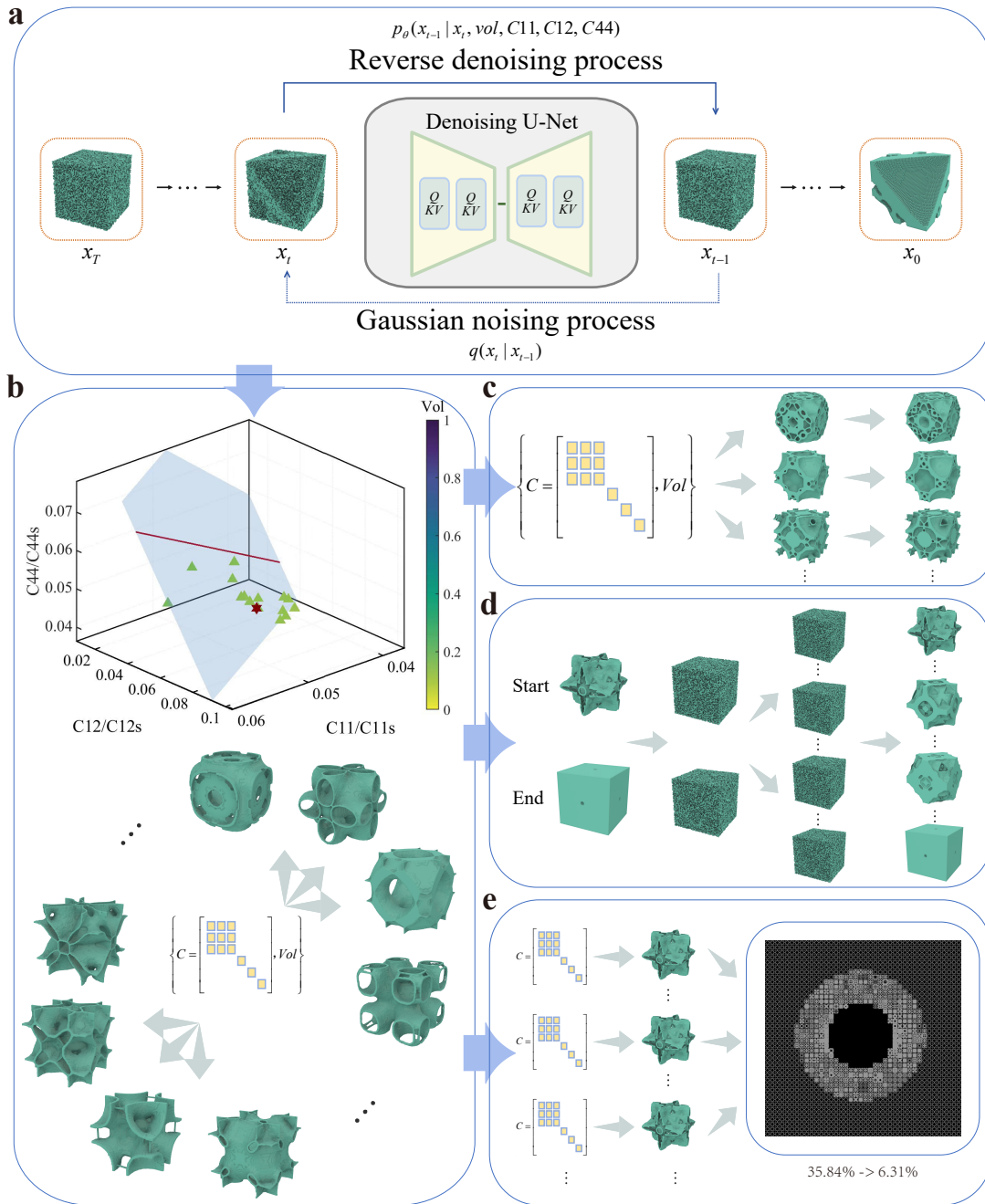


**Figure 2. Generative model framework and its three applications.** **a** Framework of the diffusion model. **b** Generation accuracy and diversity, a target elastic tensor and volume fraction as the condition of diffusion model (red hexagram in the top image) and 16 generated microstructures (green triangles in the top image, eight of which shown in the image below). **c** Using generated results as initial points of optimization. **d** Interpolation. **e** Multi-scale design.

from the previous prediction, which is introduced by self-conditioning technique<sup>44</sup>. And conditions contains elastic tensor and volume fraction, encoded by learnable sinusoidal embeddings. The loss function is as follows:

$$\mathcal{L}_{x_0} = E_{\varepsilon \sim \mathcal{N}(0,I), t \sim U(0,1)} \|f(x_t, \tilde{x}_0, t, \text{conditions}) - x_0\|_2^2. \quad (2)$$

Since the data is cubic symmetry, we force the results to be cubic symmetric at the end of the forward, which significantly improves network performance.

### Performance of diffusion model

**Fast inverse design** As voxel resolution progressively increases, computational costs will correspondingly increase via the traditional topology optimization methods. In essence, computer memory and computing time are encountering enormous challenges. After fully using hardware resources, the inverse design problem is solved by Multi-CPU framework<sup>16</sup> and GPU computation<sup>22</sup>. Nonetheless, the conventional approaches typically demand several hours for resolution. In our guided diffusion model architecture, attaining microstructures with a resolution of  $128^3$  typically requires less than 3 seconds under specified modulus.

**Accuracy and diversity** Our primary objective is to generate diverse microstructures with a prescribed elastic tensor. For accuracy assessment, we measure the relative error of the elastic tensor  $\mathbf{C}$  as the average of the relative errors associated with its three independent components, namely  $C_{11}$ ,  $C_{12}$ , and  $C_{44}$ . Error statistics are as follows

$$\text{Error}(\mathbf{C}^{\text{cond}}, \mathbf{C}^{\text{gen}}) = \frac{1}{3} \left( \left| \frac{C_{11}^{\text{cond}} - C_{11}^{\text{gen}}}{C_{11}^{\text{max}} - C_{11}^{\text{min}}} \right| + \left| \frac{C_{12}^{\text{cond}} - C_{12}^{\text{gen}}}{C_{12}^{\text{max}} - C_{12}^{\text{min}}} \right| + \left| \frac{C_{44}^{\text{cond}} - C_{44}^{\text{gen}}}{C_{44}^{\text{max}} - C_{44}^{\text{min}}} \right| \right), \quad (3)$$

where  $\mathbf{C}^{\text{cond}}$  is the target elastic tensor as the condition of the diffusion model,  $\mathbf{C}^{\text{gen}}$  is the elastic tensor of the generated structure. Figure 3b and Figure 3c show the generation accuracy on the randomly sampled test set of elasticity tensor, with an average error of 2.55%, which is further reduced to 1.74% if we choose the best structure among the four generated structures corresponding to each target tensor. From Figure 3f and Figure 2(bottom left), our diffusion model can generate a large number of differently shaped microstructures for the same target elastic tensor. For statistical analysis of diversity (and later novelty), we define a shape similarity of two microstructures  $S_1$  and  $S_2$ :

$$\text{Similarity}(S_1, S_2) = \frac{\#(\text{same voxels for } S_1 \text{ and } S_2)}{\sqrt{\#(\text{voxels in } S_1) * \#(\text{voxels in } S_2)}}, \quad (4)$$

where # is the number. In Figure 3e, we compute the pair-to-pair similarity between the four structures generated by each target tensor; the results further show that we can yield very different microstructures for the same target tensor. In all experiments in Figure 3, we set the guidance scale of the conditional diffusion model to 1, and by adjusting this guidance scale, a trade-off between accuracy and diversity can be made. It is also necessary to highlight that our model can generate results not only for a specified elastic tensor but also for a specified elastic tensor and volume fraction. Furthermore, using the classifier-guidance technique only requires training an additional regressor to enable generation under specified conditions. In our interpolation task (Figure 5), we employed a regressor predicting the ratio between the bulk modulus  $K$  and the upper limit of bulk modulus  $K_b$  under the same volume fraction, with coefficient of determination  $R^2 = 97.63\%$ . More detailed analysis is provided in supplementary materials.

**Novelty and generalizability** Additionally, our aspiration is for the model not only to memorize the training set but also to genuinely comprehend the relationships between the shape and properties of microstructures. Figure 3a compares the generated results with the training set. Our generated microstructures fill the gaps in the training set and further significantly expand the data range. To assess novelty, we continue to utilize the previously defined shape similarity in Eq. (4), and further define a similarity between a microstructure and a dataset as the maximum similarity between that structure and all microstructures in the dataset. Figure 3d illustrates the similarity between the generated results and the training set, providing evidence of our model’s ability to generate novel microstructures. In Figure 3f, we further illustrate three sets of results, comparing the generated outcomes with the microstructures in the dataset that exhibit the highest similarity. We were pleasantly surprised that most generated results were closer to the target property than their most similar microstructures in the dataset. Some exhibited noticeable shape changes, while others achieved greater proximity to the target property through subtle alterations in shape. This suggests that our model has indeed learned the relationship between the shapes of microstructures and their properties. It not only provides powerful generative capabilities but also holds the potential to assist researchers in investigating the mechanisms behind various physical properties in the future.

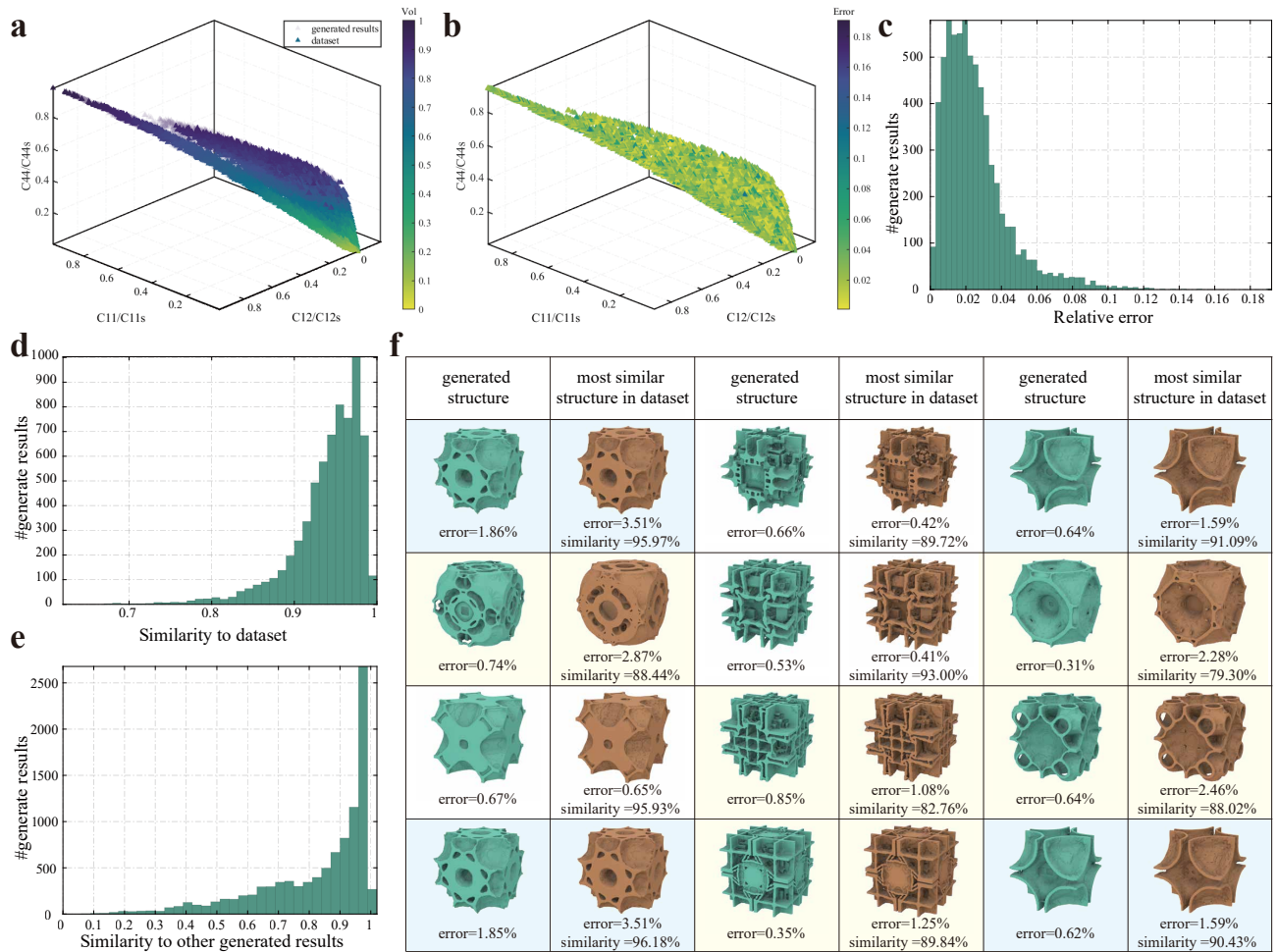
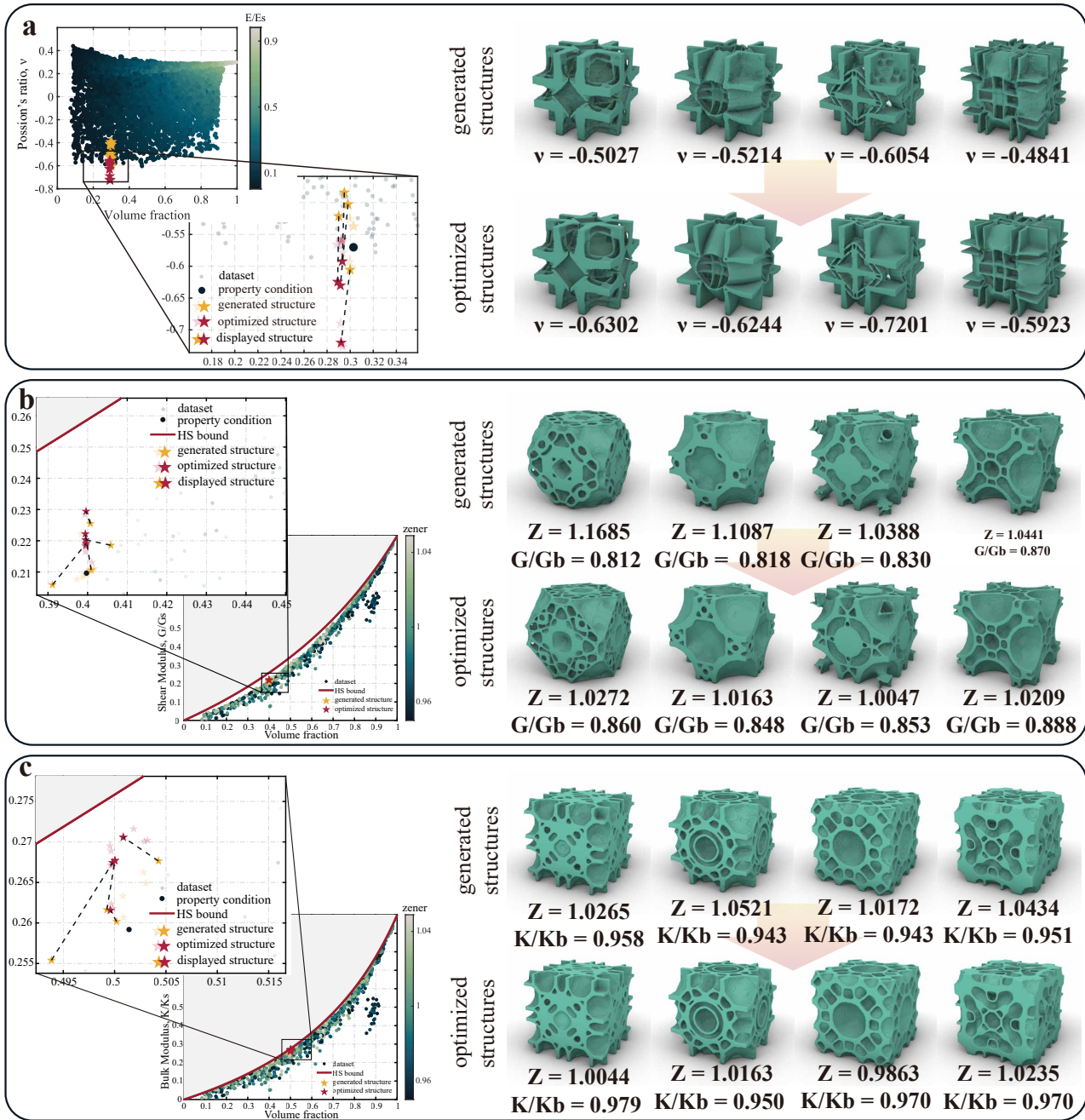


**Figure 3. Performance of the diffusion model. a-c Generalization and accuracy.** We randomly generated a total of 1660 elastic tensors in or near the dataset range, generating four structures for each elastic tensor. **a** indicates that the generated results extend the property range and fill the gap in the data set. **b** and **c** show the relative error between the generated results and their property condition. **d-f** Diversity and novelty. We describe novelty by the similarity between the generated results and the most similar structure in the dataset and show diversity by the similarity between the four structures generated by the same property condition. **f** We show three sets of structures (4 structures generated by the same condition and their most similar structures in the dataset) to demonstrate diversity and novelty further. We unexpectedly observed that the generated structures are mostly closer to the property conditions than their most similar structure in the dataset. Light yellow boxes mark the examples where the shape changes significantly and the accuracy improves. Light cyan boxes mark the examples where the shape is almost unchanged and the accuracy improves. This shows that our model does learn the relationship between shapes and properties rather than remember the dataset.

### Gradient-based optimization to approach extremum

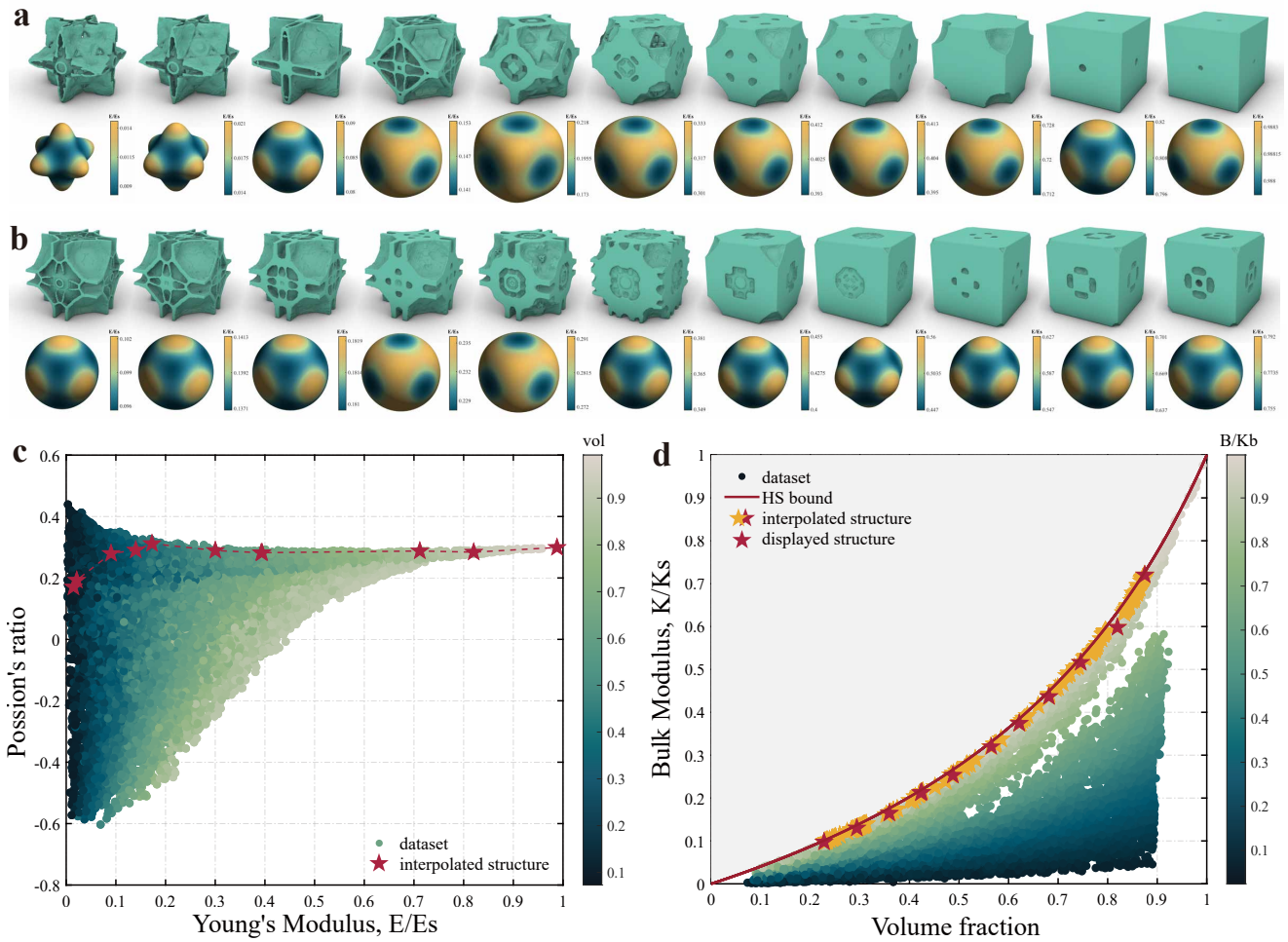
Topology optimization using high-resolution frameworks proves beneficial for exploring a broad range of metamaterials. However, it is a gradient-based optimization method whose results are closely related to the initial inputs. In other words, distinct initial values impact both the topologies and the performance of the final results. The uncertainty associated with the initial structure requires repeating the optimization process multiple times. The proposed diffusion model can provide a better initial candidate for topology optimization algorithms.

Figure 4 illustrates three cases of the optimal design of voxel-based microstructures towards extreme properties. In each of the three instances, we initially selected a microstructure from the dataset with properties close to the extreme. Using its properties as the target, we generated 16 microstructures. Our generative model produced a diverse set of initial structures near the target attributes, with some of them even surpassing the generated conditions in closeness to the extremes. This



**Figure 4. Optimization with the generated structures as the initializations.** For three challenging optimization examples (a minimizing Poisson's ratio, b maximizing shear modulus under isotropy, and c maximizing bulk modulus under isotropy), we employ our model to generate initializations to help the optimization algorithm obtain extremal and more diverse microstructures. In each example, we select a structure close to the target in the dataset and use its properties as the generation condition to generate 16 microstructures as the initial for optimization, of which four structures are shown on the right side, and their properties are shown in the zooming graph.

provides ample favorable starting points for voxel-based optimization algorithms, enabling the creation of a significant number of extreme metamaterials. In the first example, we optimized for the negative Poisson's ratio at a volume fraction of 0.3. The volume fraction and Poisson's ratio of the conditions of the diffusion model, the 16 generated results, and their corresponding optimization results are shown in Figure 4(a, left). Four sets of these microstructures are showcased on the right side of Figure 4a.



**Figure 5. Microstructure interpolation and microstructure family of extreme property.** Interpolation is done for start and end with extremely low and high Young's modulus, with resulting structures and their modulus sphere, as shown in **a**. The interpolation trajectory in the property space is shown in **c**. As a more practical example and to demonstrate controllability, we use the classifier-guidance to generate structures with bulk modulus closer to HS bound, iteratively do interpolation with interpolation results as the start and end, and finally create a family of microstructures with bulk modulus close to HS bound. Eleven representative structures and the interpolation track are shown in **b** and **d**.

We successfully optimized for a negative Poisson's ratio of -0.7437, significantly lower than the dataset's minimum value of -0.6031. Given that our dataset includes data from optimizing for negative Poisson's ratio with random initializations, this comparison indicates that the initializations generated by our model outperform random ones. In the second example (Figure 4b), optimization for shear modulus was performed under constraints of isotropy and a volume fraction of 0.4. Meanwhile, in the third example (Figure 4c), optimization was conducted on the bulk modulus under constraints of isotropy and a volume fraction of 0.5. In these two examples, we first filter out microstructures in the dataset that are close to isotropy (with a Zener anisotropy ratio greater than 0.95 and less than 1.05). Subsequently, we choose a microstructure near the corresponding volume fraction and close to HS bound, using its elastic tensor as the generation condition. We achieved structurally rich, isotropic microstructures with performance close to the HS bound. This generation-optimization approach can become a universal design process not limited by optimization goals and constraints. We can obtain richer extreme structures by selecting more generation conditions to generate more microstructures to be initial points for optimization. Additionally, we can use DDIM reverse sampling to infer noise from the optimized structure and make minor perturbations to the noise to generate a more diverse set of extreme structures.

## Microstructure interpolation

Metamaterials typically take shape through the periodic or hierarchical arrangement of individual cells. These materials must exhibit geometric connectivity<sup>25</sup> and maintain a continuous set of physical properties<sup>26</sup>. Direct generation of sequential microstructures using topology optimization methods requires extra connectivity constraints. Interpolation<sup>45</sup> is a common application in generative models and is particularly well-suited for generating sequential microstructures.

During sampling, we start with Gaussian noise and progressively denoise to obtain a clear structure. DDIM reverse sampling, on the other hand, can deduce the corresponding noise from a clear structure. From this perspective, noise can be considered as a latent space for microstructures. We perform spherical interpolation on the noise to obtain a series of continuously varying microstructures. Specifically, given the start and end structure for interpolation, we first determine their corresponding Gaussian noises, denoted as  $x_1$  and  $x_2$ . Subsequently, we generate a series of Gaussian noises  $\cos(\theta)x_0 + \sin(\theta)x_1$  where  $\theta$  sweeps from 0 to  $\frac{\pi}{2}$ . By using this series of noises for unconditional generation, a set of microstructures with continuous variations in both shape and physical properties can be obtained. Figure 5 illustrates two examples of interpolation. In the first example, we chose microstructures from the dataset with extreme Young's modulus as the start and end points. The interpolation trajectory is shown in Figure 5c, while Figure 5a displays interpolated microstructures and their modulus spheres, demonstrating a smooth transition in both shape and physical properties.

However, similar to the results in previous articles<sup>41</sup>, the interpolation trajectory obtained solely through noise interpolation is uncontrollable. The resulting microstructures cannot be directly applied to multi-scale topology optimization. Therefore, we design a family of microstructures whose bulk modulus is close to HS bound. Figure 5d illustrates the interpolation trajectory of this microstructure family, 11 selected microstructures and their modulus spheres are depicted in Figure 5b. We trained a regressor to predict the ratio of Bulk modulus to the HS bound. We then used this regressor with classifier-guidance conditions for generation, replacing the unconditional generation in the original interpolation method. This ensures that our interpolated microstructures all possess extreme Bulk modulus. Additionally, we found it challenging to obtain a dense microstructure family through a single interpolation. Even with denser interpolation points, we only get more similar microstructures, and there are always some sections cannot be filled. As a remedial measure, we initially interpolated 64 microstructures. Subsequently, we continued the interpolation using the ends of the gaps as start and end points, resulting in the interpolation of 16 additional microstructures. This iterative process was repeated until it yielded a dense microstructure family. The final microstructure family we obtained covers almost all volume fractions between the start and end points of the initial interpolation, and all microstructures possess extreme Bulk modulus.

## Multiscale design

To exemplify our proposed method, we employ voxel-based datasets to design mechanical cloak multiscale systems applications. The reference structures (absent voids and cloak) consist of  $40 \times 40 \times 40$  periodically tessellated base cells selected from the metamaterials dataset. We design the invisibility cloak for two situations: (1) The first case involves excising a cylinder with a radius of  $\frac{20}{3}$ , and subsequently filling the outer circular region (comprising a cylinder with an outer radius of  $\frac{40}{3}$ ) with material to achieve the design of the invisibility cloak. (2) the second case, the cylinder from the first case is substituted with a rectangular column. The cross-sectional shape of this column is a square with a side length equal to the diameter of the original cylinder. Simultaneously, we explored applying two distinct reference structures: one characterized by a plate structure with a thickness of eight voxels on each face and the other representing an isotropic structure identified from the dataset to emulate materials with isotropic properties. The effectiveness of the cloak's stealth capabilities is considered superior when the discrepancy between the displacement and the reference displacement is minimized. In all four instances, a noteworthy reduction in displacement distortion was achieved.

## Discussion

This paper introduces a novel and efficient solution through a fast inverse design method leveraging an advanced deep generative AI algorithm. The core of this approach is the self-conditioned diffusion model, a powerful tool capable of generating voxel-based mechanical metamaterials with a resolution as high as  $128^3$ . What sets our method apart is its remarkable ability to approach the specified homogenized tensor matrix in 3 seconds. The immediate application of this rapid reverse design tool is evident in its capability to facilitate the exploration of extreme metamaterials. By providing a quick and efficient means to generate metamaterial structures, our approach allows for sequence interpolation in metamaterials, opening avenues for designing materials with tailored mechanical responses. Furthermore, the tool enables the generation of diverse microstructures, facilitating multi-scale design considerations.

In the realm of structural engineering and other mechanical systems, the flexibility and adaptability of our generative tool hold immense value. Beyond the immediate applications discussed, the tool is expected to stimulate further research by providing researchers with a swift and efficient means of exploring and testing novel mechanical metamaterial designs. In conclusion, our proposed fast inverse design method, driven by an advanced deep generative AI algorithm, represents a

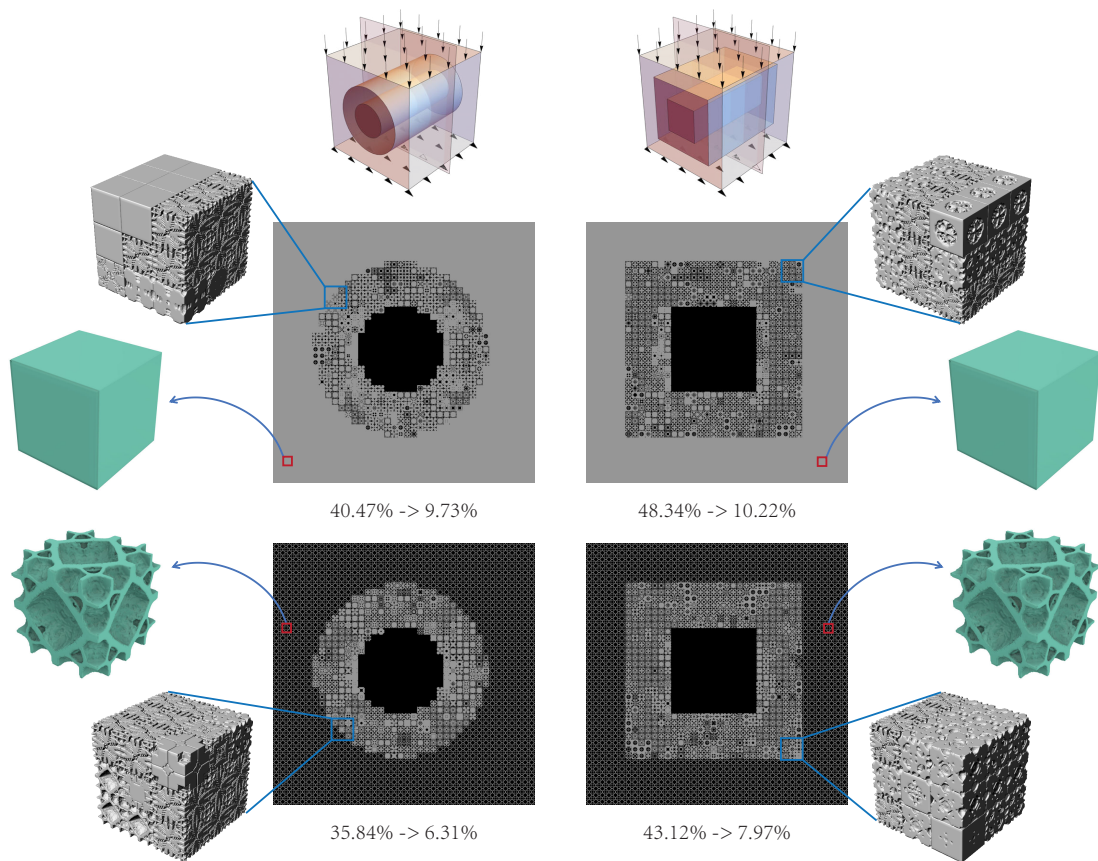


**Figure 6. Mechanical cloak via multi-scale design.** Four mechanical invisibility cloaks. The left two consider cutting out a cylinder in a cube and designing an invisibility cloak around it. The right two cut out a rectangular column in the cube and design an invisibility cloak around it. Middle sections and local  $3 \times 3 \times 3$  structures are rendered. The cyan structures are the reference structures.

significant advancement in the field of mechanical metamaterials. Its capabilities offer not only immediate practical applications but also the potential to inspire and drive future research endeavors in materials science and engineering.

## Methods

### Data generation

**Data format** All density-based microstructures are obtained by the inverse homogenization method in a cube domain. The cube is discretized into  $n$  voxel elements, with each element assigned a density value of 0 (void) or 1 (solid). Various combinations of 0 and 1 give rise to different microstructures, totaling  $2^n$  combinations. The number of microstructure variations expands exponentially with the resolution parameter,  $n$ . Consequently, voxel-based representations exhibit significant representational capabilities. However, it is important to note that not all combinations yield satisfactory microstructures, and the huge amount of data may impose a considerable burden on subsequent training and machine learning algorithms. When constructing the data set, we take into account the cube symmetry employing the  $\frac{1}{8}$  unit cell lattice to simplify the representation. Subsequently, symmetric operations are applied to the  $\frac{1}{8}$  unit cell lattice. This process ultimately leads to a cubic symmetric microstructure to facilitate calculation. To create a sufficiently large design space for a metamaterial database based on voxels, we establish microstructures at a resolution of  $128^3$  and subsequently store  $\frac{1}{8}$ -th of it, equivalent to  $64^3$  microstructures.

**Extension from perturbation data** Our perturbation algorithm is an iterative process wherein, at each step, we locally apply elastic deformation to specified structures. The deformation field is characterized by random Gaussian noise. Initially, this perturbation is broadly applied to the entire dataset. As the iterations progress, each subsequent step specifically targets a range of Poisson's ratio that is underrepresented in the current dataset. This targeted approach enables us to concentrate the perturbation on areas where modulus coverage is less extensive, thereby enhancing the dataset's diversity in these particular

aspects. Through continuously adjusting our focus to different Poisson's ratio ranges with each iteration, we gradually achieve a dataset with a broad and comprehensive range of modulus coverage.

**Data statistics** The objective functions for optimization are the bulk modulus, shear modulus, and Poisson's ratio. We impose volume constraints during the optimization process. The total optimization results consist of 10,000 structures for volume modulus and shear modulus, while 5,000 structures are obtained for Poisson's ratio. The volume fractions considered in the optimization range from 0.2 to 0.9. In utilizing the iterative perturbation method, a total of 60,000 structures were initially generated. Following the removal of disconnected portions within the microstructure, as illustrated in Figure 1, 74,717 microstructures remained. To enhance training efficiency, a subset of 10,000 data was uniformly selected from the original dataset comprising 74,717 entries.

### Framework of diffusion model

The backbone denoising network is an U-Net based on the standard 3D convolutional neural network. Following LAS-Diffusion<sup>46</sup>, the U-Net is composed of 5 levels:  $64^3$ ,  $32^3$ ,  $16^3$ ,  $8^3$ , and  $4^3$ , with feature dimensions gradually increasing to 32, 64, 128, 256, and 256, respectively. Each level is constructed with a ResNet block, which includes two convolution layers with a kernel size of 3. In the U-Net's bottleneck, two ResNet blocks are introduced. To map the voxel features at the finest level to a surface-occupancy value, a convolution layer is added at the conclusion of the network.

### References

1. Meza, L. R. *et al.* Resilient 3d hierarchical architected metamaterials. *Proc. Natl. Acad. Sci.* **112**, 11502–11507 (2015).
2. Jiang, Y. & Wang, Q. Highly-stretchable 3d-architected mechanical metamaterials. *Sci. reports* **6**, 34147 (2016).
3. Surjadi, J. U. *et al.* Mechanical metamaterials and their engineering applications. *Adv. Eng. Mater.* **21**, 1800864 (2019).
4. Chen, Y., Li, T., Scarpa, F. & Wang, L. Lattice metamaterials with mechanically tunable poisson's ratio for vibration control. *Phys. Rev. Appl.* **7**, 024012 (2017).
5. Li, T., Hu, X., Chen, Y. & Wang, L. Harnessing out-of-plane deformation to design 3d architected lattice metamaterials with tunable poisson's ratio. *Sci. Reports* **7**, 8949 (2017).
6. Khan, K. A., Alshaer, M. H. & Khan, M. A. A novel twofold symmetry architected metamaterials with high compressibility and negative poisson's ratio. *Adv. Eng. Mater.* **23**, 2001041 (2021).
7. Farzaneh, A., Pawar, N., Portela, C. M. & Hopkins, J. B. Sequential metamaterials with alternating poisson's ratios. *Nat. communications* **13**, 1041 (2022).
8. Zhang, J., Xiao, M., Gao, L., Alù, A. & Wang, F. Self-bridging metamaterials surpassing the theoretical limit of poisson's ratios. *Nat. Commun.* **14**, 4041 (2023).
9. Ghaedizadeh, A., Shen, J. H., Ren, X. & Xie, Y. M. Geometric bounds for buckling-induced auxetic metamaterials undergoing large deformation. *Appl. Mech. Mater.* **846**, 547–552 (2016).
10. Yang, H. & Ma, L. Multi-stable mechanical metamaterials by elastic buckling instability. *J. materials science* **54**, 3509–3526 (2019).
11. Yves, S. *et al.* Crystalline metamaterials for topological properties at subwavelength scales. *Nat. communications* **8**, 16023 (2017).
12. Bertoldi, K., Vitelli, V., Christensen, J. & Van Hecke, M. Flexible mechanical metamaterials. *Nat. Rev. Mater.* **2**, 1–11 (2017).
13. Yu, X., Zhou, J., Liang, H., Jiang, Z. & Wu, L. Mechanical metamaterials associated with stiffness, rigidity and compressibility: A brief review. *Prog. Mater. Sci.* **94**, 114–173 (2018).
14. Jiao, P., Mueller, J., Raney, J. R., Zheng, X. & Alavi, A. H. Mechanical metamaterials and beyond. *Nat. Commun.* **14**, 6004 (2023).
15. Hassani, B. & Hinton, E. A review of homogenization and topology optimization i—homogenization theory for media with periodic structure. *Comput. & Struct.* **69**, 707–717 (1998).
16. Aage, N., Andreassen, E. & Lazarov, B. S. Topology optimization using petsc: An easy-to-use, fully parallel, open source topology optimization framework. *Struct. Multidiscip. Optim.* **51**, 565–572 (2015).
17. Borrvall, T. & Petersson, J. Large-scale topology optimization in 3d using parallel computing. *Comput. methods applied mechanics engineering* **190**, 6201–6229 (2001).

18. Aage, N., Andreassen, E., Lazarov, B. S. & Sigmund, O. Giga-voxel computational morphogenesis for structural design. *Nature* **550**, 84–86 (2017).
19. Challis, V. J., Roberts, A. P. & Grotowski, J. F. High resolution topology optimization using graphics processing units (gpu). *Struct. Multidiscip. Optim.* **49**, 315–325 (2014).
20. Xia, Z., Wang, Y., Wang, Q. & Mei, C. Gpu parallel strategy for parameterized lsm-based topology optimization using isogeometric analysis. *Struct. Multidiscip. Optim.* **56**, 413–434 (2017).
21. Wu, J., Dick, C. & Westermann, R. A system for high-resolution topology optimization. *IEEE transactions on visualization computer graphics* **22**, 1195–1208 (2015).
22. Zhang, D., Zhai, X., Liu, L. & Fu, X.-M. An optimized, easy-to-use, open-source gpu solver for large-scale inverse homogenization problems. *Struct. Multidiscip. Optim.* **66**, 207 (2023).
23. Stainko, R. An adaptive multilevel approach to the minimal compliance problem in topology optimization. *Commun. numerical methods engineering* **22**, 109–118 (2006).
24. Wang, S., de Sturler, E. & Paulino, G. H. Dynamic adaptive mesh refinement for topology optimization. *arXiv preprint arXiv:1009.4975* (2010).
25. Du, Z., Zhou, X.-Y., Picelli, R. & Kim, H. A. Connecting microstructures for multiscale topology optimization with connectivity index constraints. *J. Mech. Des.* **140**, 111417 (2018).
26. Garner, E., Kolken, H. M., Wang, C. C., Zadpoor, A. A. & Wu, J. Compatibility in microstructural optimization for additive manufacturing. *Addit. Manuf.* **26**, 65–75 (2019).
27. Lee, D., Chen, W., Wang, L., Chan, Y.-C. & Chen, W. Data-driven design for metamaterials and multiscale systems: A review. *Adv. Mater.* 2305254 (2023).
28. Zeng, Q., Zhao, Z., Lei, H. & Wang, P. A deep learning approach for inverse design of gradient mechanical metamaterials. *Int. J. Mech. Sci.* **240**, 107920 (2023).
29. Zheng, X., Zhang, X., Chen, T.-T. & Watanabe, I. Deep learning in mechanical metamaterials: From prediction and generation to inverse design. *Adv. Mater.* 2302530 (2023).
30. Zheng, X., Chen, T.-T., Guo, X., Samitsu, S. & Watanabe, I. Controllable inverse design of auxetic metamaterials using deep learning. *Mater. & Des.* **211**, 110178 (2021).
31. Kumar, S., Tan, S., Zheng, L. & Kochmann, D. M. Inverse-designed spinodoid metamaterials. *npj Comput. Mater.* **6**, 73 (2020).
32. Patel, D., Bielecki, D., Rai, R. & Dargush, G. Improving connectivity and accelerating multiscale topology optimization using deep neural network techniques. *Struct. Multidiscip. Optim.* **65**, 126 (2022).
33. Seo, M. & Min, S. DI-msto+: A deep learning-based multi-scale topology optimization framework via positive definiteness ensured material representation network. *Comput. Methods Appl. Mech. Eng.* **415**, 116276 (2023).
34. Jiao, P. & Alavi, A. H. Artificial intelligence-enabled smart mechanical metamaterials: advent and future trends. *Int. Mater. Rev.* **66**, 365–393 (2021).
35. Song, J., Lee, J., Kim, N. & Min, K. Artificial intelligence in the design of innovative metamaterials: A comprehensive review. *Int. J. Precis. Eng. Manuf.* 1–20 (2023).
36. Wang, L., Chan, Y.-C., Liu, Z., Zhu, P. & Chen, W. Data-driven metamaterial design with laplace-beltrami spectrum as “shape-dna”. *Struct. multidisciplinary optimization* **61**, 2613–2628 (2020).
37. Chan, Y.-C., Ahmed, F., Wang, L. & Chen, W. Metaset: Exploring shape and property spaces for data-driven metamaterials design. *J. Mech. Des.* **143**, 031707 (2021).
38. Lee, D. *et al.* t-METASET: Task-Aware Acquisition of Metamaterial Datasets Through Diversity-Based Active Learning. *J. Mech. Des.* **145**, 031704, [10.1115/1.4055925](https://doi.org/10.1115/1.4055925) (2022). [https://asmedigitalcollection.asme.org/mechanicaldesign/article-pdf/145/3/031704/6938884/md\\_145\\_3\\_031704.pdf](https://asmedigitalcollection.asme.org/mechanicaldesign/article-pdf/145/3/031704/6938884/md_145_3_031704.pdf).
39. Korshunova, N., Papaioannou, I., Kollmannsberger, S., Straub, D. & Rank, E. Uncertainty quantification of microstructure variability and mechanical behavior of additively manufactured lattice structures. *Comput. Methods Appl. Mech. Eng.* **385**, 114049 (2021).
40. Bastek, J.-H., Kumar, S., Telgen, B., Glaesener, R. N. & Kochmann, D. M. Inverting the structure–property map of truss metamaterials by deep learning. *Proc. Natl. Acad. Sci.* **119**, e2111505119 (2022).

41. Zheng, L., Karapiperis, K., Kumar, S. & Kochmann, D. M. Unifying the design space and optimizing linear and nonlinear truss metamaterials by generative modeling. *Nat. Commun.* **14**, 7563 (2023).
42. Simard, P. Y., Steinkraus, D., Platt, J. C. *et al.* Best practices for convolutional neural networks applied to visual document analysis. In *Icdar*, vol. 3 (Edinburgh, 2003).
43. Simard, P., Steinkraus, D. & Platt, J. Best practices for convolutional neural networks applied to visual document analysis. In *Seventh International Conference on Document Analysis and Recognition, 2003. Proceedings.*, 958–963, [10.1109/ICDAR.2003.1227801](https://doi.org/10.1109/ICDAR.2003.1227801) (2003).
44. Chen, T., Zhang, R. & Hinton, G. Analog bits: Generating discrete data using diffusion models with self-conditioning. *arXiv preprint arXiv:2208.04202* (2022).
45. Dhariwal, P. & Nichol, A. Diffusion models beat gans on image synthesis. *Adv. neural information processing systems* **34**, 8780–8794 (2021).
46. Zheng, X.-Y. *et al.* Locally attentional sdf diffusion for controllable 3d shape generation. *arXiv e-prints arXiv-2305* (2023).